ACS SENSORS

Article

pubs.acs.org/acssensors

Interfacial Donor–Acceptor Nanofibril Composites for Selective Alkane Vapor Detection

Chen Wang,[†] Benjamin R. Bunes,[†] Miao Xu,[†] Na Wu,[†] Xiaomei Yang,[†] Dustin E. Gross,[‡,§] and Ling Zang*[,†]

[†]Nano Institute of Utah and Department of Materials Science and Engineering, University of Utah, Salt Lake City, Utah 84112, United States

[‡]Department of Chemistry, University of Illinois at Urbana–Champaign, Urbana, Illinois 61801, United States

Supporting Information

ABSTRACT: The detection of alkane vapors has strong implications for safety, health, and the environment. Alkanes are notoriously difficult to detect because of their chemical inertness at room temperature. Herein, we introduce a tunable photoinduced charge transfer strategy to selectively detect alkane vapors under ambient condition. A unique donor–acceptor nanofibril composite comprising a compatible interface was fabricated, which is preferential for alkane adsorption. Then the enhanced adsorption disrupts the charge transfer across the interface and decreases the photocurrent, enabling the design of alkane gas sensor. We demonstrate a critical relationship between the tunable donor–acceptor interface and alkane response. The composite sensor is able to provide specific distinction between different alkanes based on their kinetics of the response profiles, and outstanding general selectivity against the common polar solvents. The work described herein may provide a basis for a new type of sensing material for detecting inert chemicals at room temperature.

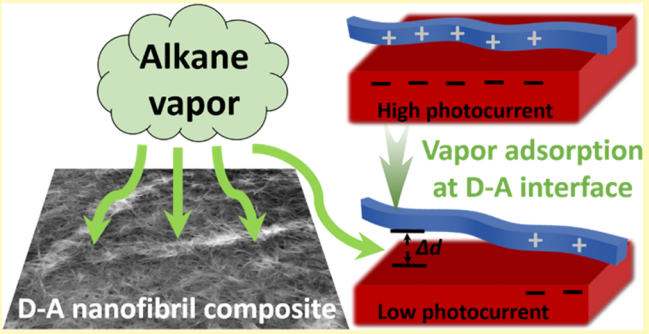

KEYWORDS: *alkane detection, tunable D–A interface, photoinduced charge transfer, nanofiber composite, interfacial engineering*

Alkanes are primary energy sources, important industrial crude materials, and solvents for modern society. While serving people, they also pose risks to security, the environment, and human health. For example, alkane vapors and the ammonium nitrate fuel oil mixture (ANFO) are extremely explosive, and have brought numerous disasters in recent years.[1−4] Besides, alkane vapors are proven to cause systemic toxicity to the human nervous system.[5−7] A reliable, quick, and portable detection method for alkane vapor is necessary for industrial control and public safety. However, current technologies still face great challenges in alkane vapor detection, particularly with trace level sensitivity and real-time monitoring. Traditional instrumentation, such as gas chromatography coupled with mass spectrometry or photoionization detection, and ion mobility spectrometry, are often slow, expensive, and not sufficiently selective.[8] On the other hand, the chemical inertness of alkanes hinders the design of reaction-based chemical sensors. To initiate the sensing reactions, some sensors have to be operated at an elevated temperature (>400 °C) at the expense of selectivity, portability, and power consumption.[9] At the low temperature range, the intermolecular interaction with alkanes is dominated by the van der Waals force. Therefore, we determined that the key for the development of room temperature alkane sensors is to optimize the van der Waals interaction between alkanes and sensor materials and to transmit the interaction process into a measurable physical quantity.

Herein, we report an approach based on the tunable photoinduced charge transfer (PCT) process in an organic nanofibril donor–acceptor (D–A) composite. It has a unique D–A interface composed of interdigitated soft alkyl chains, with large surface area and three-dimensional porosity, which provides the preferential adsorption for alkanes through solvophilic (van der Waals) interaction into the D–A interface. Since the PCT efficiency is sensitive to the slight distance change, the adsorbed alkanes at the D–A interface are expected to be able to fractionally interrupt the original interfacial interdigitation, leading to an overall distance increase, which weakens the PCT and, thus, decreases the electrical conductivity.[10−14] To achieve the desired structure and the sensing ability, the building-block molecules for the D–A composites are selected as a long alkyl-substituted arylene-ethynylene tetracycle (ACTC) as the donor (Figure 1a), and perylene-3,4,9,10-tetracarboxylic-3,4,9,10-diimide (PTCDI) modified with different side chains, dodecyl (-DD), cyclohexyl (-C_6), and propoxyethyl (-PE), as the acceptors (Figure 1b).

Received: January 10, 2016
Accepted: March 9, 2016
Published: March 9, 2016

DOI: 10.1021/acssensors.6b00018
ACS Sens. 2016, 1, 552–559

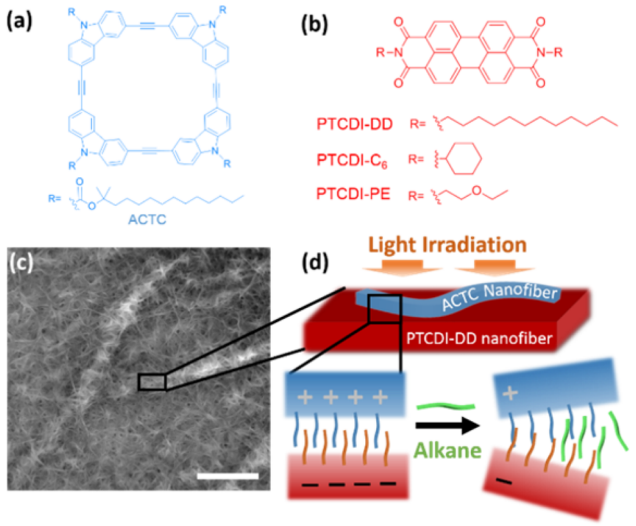

Figure 1. Molecular structures of (a) ACTC and (b) end-substituted PTCDI molecules, PTCDI-DD, PTCDI-C_6, and PTCDI-PE. (c) SEM image of ACTC/PTCDI-DD nanofibril composite with large number of ultrathin ACTC fibers attached onto the larger PTCDI fibers; scale bar = 3 μm. (d) Scheme showing the alkane sensing mechanism based on the tunable PCT process at D−A interface.

Through molecular coassembly in solution, three fibril composites, ACTC/PTCDI-DD, ACTC/PTCDI-C_6, and ACTC/PTCDI-PE, were fabricated and showed significant difference in the D−A interfaces, resulting in a large divergence in photocurrent generation and the corresponding sensing performance. Among them, ACTC/PTCDI-DD, which is a bulk-heterojunction from homogeneously coassembled PTCDI-DD and ACTC nanofibers (Figure 1c), showed the best sensing performance for alkanes. According to the control experiments, we confirmed that besides the compatible surface for alkane absorption on the molecular level, the availability of adsorbed alkanes to tune the D−A interface is another necessary feature for the successful detection of alkanes, on the structural level. By monitoring the photocurrent change upon exposure, alkanes can be detected and further distinguished in different molecular sizes based on their unique kinetics of absorption and disassociation. Moreover, the sensor provides opposite response trends to alkanes over common polar solvents, which leads to good general selectivity for real world applications. Through these investigations, we proved the critical role of tunable D−A interface in the process of alkane detection and our work extended the concept of organic D−A heterojunctions to a design strategy for novel chemical sensors.[15−21]

Nanofibers comprising PTCDI-DD, PTCDI-C_6, and PTCDI-PE were fabricated via a previously reported solution-based self-assembly method, respectively.[22] These nanofibers are tens of micrometers long and hundreds of nanometers wide (Figure 2a,d,g, and Figure S2a,c,e). Their structures are rigid without significant bending or intertwining. The one-dimensional growth of these fibril structures results from the strong

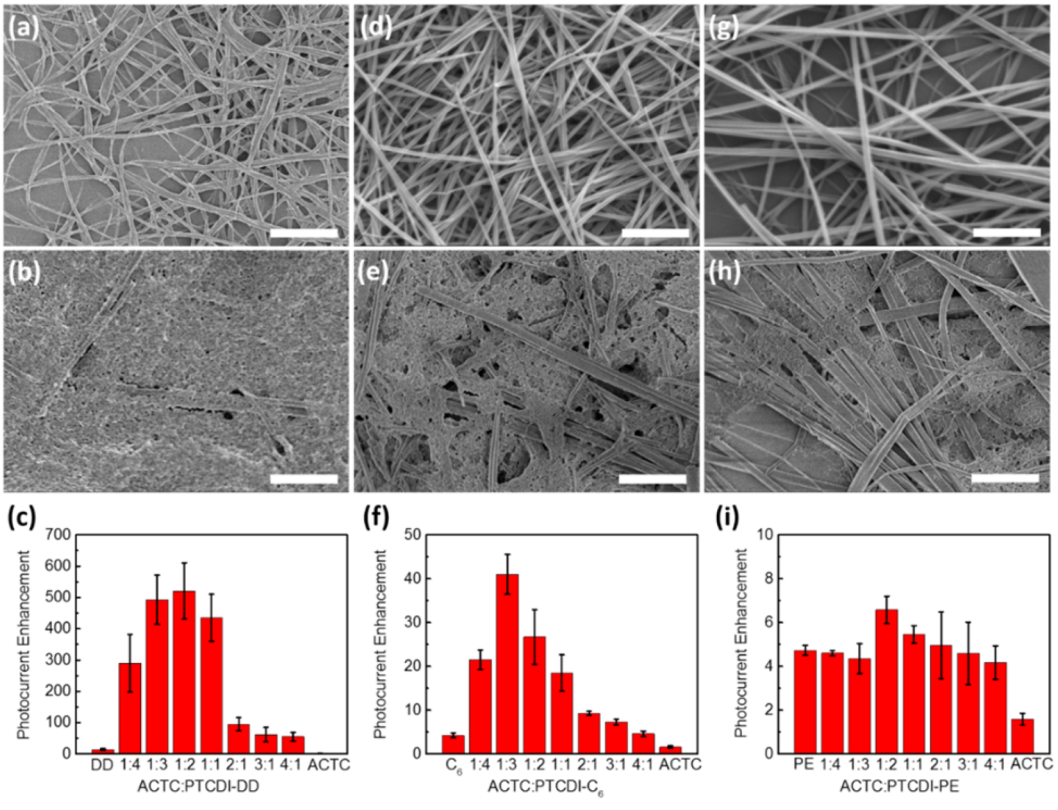

Figure 2. SEM images of (a) PTCDI-DD nanofibers and (b) ACTC/PTCDI-DD nanofibril composite; (d) PTCDI-C_6 nanofiber and (e) ACTC/PTCDI-C_6 nanofibril composite; (g) PTCDI-PE nanofibers and (h) ACTC/PTCDI-PE nanofibril composite. Scale bar = 5 μm. The statistical photocurrent enhancement measured for the three nanofibril composites, (c) ACTC/PTCDI-DD, (f) ACTC/PTCDI-C_6, and (i) ACTC/PTCDI-PE, depending on the molar ratio of ACTC to PTCDI in the precursor solutions used to fabricate the nanofibril composite through the coassembly method.

DOI: 10.1021/acssensors.6b00018
ACS Sens. 2016, 1, 552−559

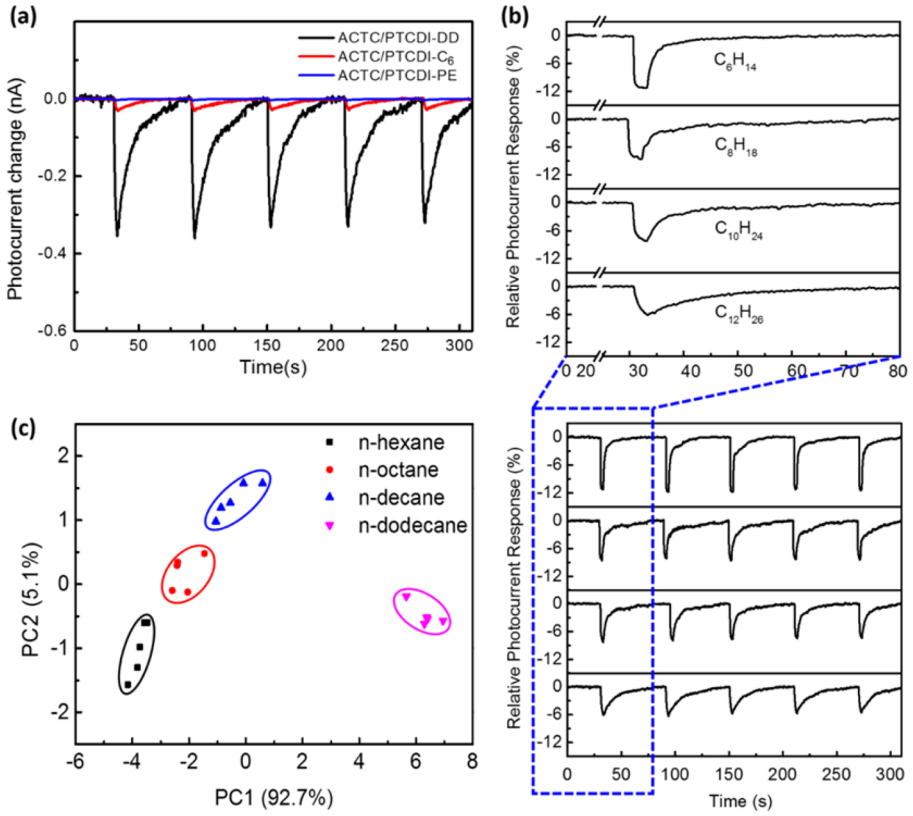

Figure 3. (a) Photocurrent change (baseline corrected) comparison upon a saturated *n*-dodecane vapor exposure of ACTC/PTCDI-DD (black), ACTC/PTCDI-C_6 (red), and ACTC/PTCDI-PE (blue) composites at room temperature. (b) Relative photocurrent response (baseline corrected) of ACTC/PTCDI-DD (ACTC:PTCDI-DD ratio is 1:2) composite to time curves measured at room temperature for saturated vapors of *n*-hexane (C_6H_{14}, 1.6×10^5 ppm), *n*-octane (C_8H_{18}, 1.0×10^4 ppm), *n*-decane ($C_{10}H_{22}$, 2.1×10^3 ppm), and *n*-dodecane ($C_{12}H_{26}$, 2.2×10^2 ppm) (from top to bottom). The relative photocurrent response is defined as $(1 - I_t/I_0) \times 100\%$, where I_t is the photocurrent at time t; I_0 is the photocurrent at the time zero. (c) Principal component scores for the responses of four alkanes exposures (5 trials for each alkane); the colored circles present the clustering results for the four alkanes.

$\pi-\pi$ stacking interaction between PTCDI skeletons along the long axial direction, which is dominant over the relatively weak interaction in the lateral direction.[23,24] The extended $\pi-\pi$ stacking results in effective π-electron delocalization, which in turn leads to enhanced charge migration along the nanofiber's backbone.[25−27] The end-substituted groups (-DD, -C_6, and -PE) comprise the surface of the PTCDI nanofibers. In comparison, the nanofibers assembled from ACTC molecules are much thinner (Figure S1), consistent with a previously reported result.[28] These nanofibers are several micrometers long and tens of nanometers wide. They twisted and merged to form a spatial network with nanometer-size porosity, which make the ACTC nanofibers relatively soft and fluffy, ensuring the ease of the D−A distance changing after alkane adsorption. Meanwhile, the much smaller size of the ACTC fibers is conducive to constructing a large area D−A interface area by allowing more ACTC fibers to attach to the surface of the PTCDI fiber, as illustrated in Figure 1c. A large D−A interface is important for efficient photoinduced charge separation, as demonstrated in numerous bulk-heterojunction photovoltaics.

By coassembling PTCDI and ACTC molecules in an appropriate solvent, nanofibril composites with varying interfacial contact were obtained between the two nanofibers depending on the side groups (Figure 2b,e,h). In these composites, the ACTC and PTCDI nanofibers maintained similar morphologies as when they are fabricated separately. In the ACTC/PTCDI-DD composite, the ACTC nanofibers were homogeneously spread over the much larger PTCDI fibers, forming a continuous nanofibril network (porous film). The composite film possessed few gaps and cracks as shown in the large-area SEM image (Figure 2b). The good dispersion of ACTC nanofibers on the PTCDI-DD is primarily due to the hydrophobic interdigitation between the long alkyl chains of ACTC and PTCDI-DD.[17,27] Such a composite is considered to be a cooperative self-assembly rather a simple self-sorting.[29] In contrast to the ACTC/PTCDI-DD, the ACTC/PTCDI-C_6 film showed less uniformity, indicating relatively poor interfacial contact between ACTC and PTCDI-C_6 nanofibers (Figure 2e). This is attributed to the weaker attraction between linear alkyl chains and cyclohexyl groups. The ACTC/PTCDI-PE film showed an almost complete phase separation with little interfacial contact between ACTC and PTCDI-PE nanofibers owing to the incompatibility of hydrophilic propoxyethyl chains to alkyl chains (Figure 2h). Such morphological differences are also confirmed by optical microscopy images (Figure S2). On the other hand, we confirmed from the absorption spectra of the composites that no charge transfer band is observed in the longer wavelength range (Figure S3), which typically indicates the formation of a steady-state charge transfer complex.[30]

With the structures determined, we turned our investigation to the photocurrent generation of nanofibril composites. First, we evaluated the dependence of the photocurrent enhancement (defined as the ratio of the current under illumination to the current in the dark for each device, I_{photo}/I_{dark}) on the molar

DOI: 10.1021/acssensors.6b00018
ACS Sens. 2016, 1, 552−559

ratio of ACTC to PTCDI to study the maximum levels of photoconductivity for the three composites (Figure 2c,f,i). All $I-V$ curves of the composites display approximately linear behavior (Figure S4), indicating that the density of trap states is low. Although the calculated energy levels of ACTC and PTCDIs indicate a similar driving force for the PCT process in all three composites (Figure S5), the maximum photocurrent enhancement is quite different over the composites due to the different D−A interface, with ACTC/PTCDI-DD and ACTC/PTCDI-C_6 composites showing a clear maximum. Increasing the amount of ACTC nanofibers present increases the D−A interfacial area and, thus, enhances the photocurrent. On the other hand, too much ACTC, which is highly resistive, blocks the percolation pathways, resulting in a decrease in conductivity. Thus, an optimal molar ratio of ACTC to PTCDI was observed for both composites. The ACTC/PTCDI-DD composite showed an enhancement 1 order of magnitude larger than the ACTC/PTCDI-C_6 composite. This is attributed to the improved interfacial contact as observed during the morphology study. By contrast, the photocurrent enhancement of the ACTC/PTCDI-PE composite is similar to the pristine PTCDI-PE and showed a negligible dependence on molar ratio due to the lack of interfacial contact between the two materials. The photocurrent enhancement data also correlate well with the yields of fluorescence quenching in the three composites (Figures S6 and S7), which indicates that the difference in photocurrent enhancement indeed arises from the divergence of PCT efficiencies by morphological reason.

As we postulated, the favorable adsorption of alkanes at the interface results in an increased D−A distance, which is evidenced as a decrease in photocurrent. To verify this mechanism, the photocurrent responses of the three ACTC/PTCDI composites (at their optimal ACTC to PTCDI molar ratios) were compared upon the exposure to a saturated vapor of *n*-dodecane at room temperature. A rapid decrease in photocurrent was observed upon exposure, followed by a relatively slow recovery after removing the analyte source for all three ACTC/PTCDI composites (Figure 3a). Among them, the ACTC/PTCDI-DD composite showed the largest photocurrent change, which is over ten times greater than ACTC/PTCDI-C_6 and over two hundred times greater than ACTC/PTCDI-PE. This order of difference correlates closely with the estimated PCT efficiencies due to their common origin, the D−A interface. For the ACTC/PTCDI-DD composite, the donor and acceptor nanofibers are interconnected by flexible alkyl chains, which is very similar to the alkane molecules. One would expect a favorable adsorption at the interface (following the common chemistry principle, "like dissolves like"), leading to a high local concentration of alkanes. The flexibility of the alkyl chains at the interface provides freedom of movement for the D−A distance upon the adsorption and diffusion of alkane molecules at the interface.[31,32] Although this movement is in the submolecular distance range, it is enough to sufficiently interfere with the PCT efficiency.[17] In ACTC/PTCDI-C_6, the PCT efficiency is moderate due to the partially formed D−A interface, and its response, as expected is moderate. In ACTC/PTCDI-PE, the lack of an alkyl-compatible D−A interface results in the lowest response, even though the phase separated ACTC nanofibers themselves should still adsorb alkane molecules, whereas, without the efficient PCT process, the observation of a photocurrent response to alkane vapors would be difficult. Additionally, the large photocurrent caused by the high PCT efficiency is desired for chemiresistive sensing materials, which may enlarge the potential detectable concentration range and lower the detection limit with an enhanced signal/noise ratio. Consequently, the interface morphology is closely linked to the sensor performance.

To further verify the high sensitivity ACTC/PTCDI-DD composite toward alkanes, the composite was also exposed to the saturated vapors of *n*-hexane, *n*-octane, and *n*-decane. Overall, the composite responded to alkane exposures with photocurrent decrease in different yields. The saturated hexane vapor provided about 12% photocurrent reduction, and with the increasing alkane length, less reduction was observed (for example, 6% for dodecane) (Figure 3b). Generally, as the vapor was diluted, the amplitudes of photocurrent response decreased. When the alkane vapors were diluted to 1% of their saturated concentrations, the responses of the composite still remained at least seven times larger than the general noise level of the baseline (Figure S8). Based on the criteria that the signal-to-noise ratio is greater than 3, the limit of detection (LOD) is below these concentrations. We expect that the LOD can be significantly lowered if the detection system is further optimized through professional engineering.

Furthermore, it is interesting to see from Figure 3b that the response profiles for alkanes show dramatically different kinetics during and after exposures. This difference enabled us to classify different analytes within the series of alkanes. When the sensor was initially exposed to an analyte, the photocurrent of the composite immediately started a rapid decrease, indicating the alkanes began to be adsorbed and to interrupt the PCT process. After this stage, the rates of photocurrent decreasing behave differently according to each alkane. Figure 3b shows the relative photocurrent responses upon five exposures of the four alkanes, along with the time-magnified curves for the first exposures. For the *n*-hexane, after the rapid decrease, a stage with relatively stable photocurrent was reached during the exposure. Due to the weak interaction and low molecular weight, the average staying time at the interface is low for short chain alkanes. This stage may imply a quasi-equilibrium state between alkane molecule adsorption and disassociation from the surface.[33] These steady stages gradually disappeared with the increasing length of alkane molecules. For *n*-dodecane, such stages totally disappeared, due to the stronger interaction with the alkyl interface, which makes the disassociation rate slower than the adsorption rate during the exposure period. The longer staying time may allow larger alkanes to diffuse deeper into ACTC/PTCDI-DD interface. Additionally, because of their larger size, the interruption to the photocurrent should be more effective at the D−A interface. So we attribute the larger current decrease observed for *n*-hexane than the other normal alkanes to its higher vapor concentration. Consistently, if all alkanes are produced at the same concentration, the longer alkanes will cause larger photocurrent changes. For example, a saturated vapor of *n*-dodecane has a comparable vapor concentration as the 1% dilution of *n*-hexane, but the former produces about one magnitude of order higher response than the latter (Figure S8a and d). It should be noted that the analytes are not limited to normal alkanes. For example, cycloalkane vapor is also detectable due to the same adsorption mechanism (see Figure S9 for saturated cyclohexane vapor). Due to the bulkier conformation compared *n*-hexane, the saturated vapor of cyclohexane caused a larger decrease than *n*-hexane at similar vapor concentrations.

After exposure, the photocurrent recovered at different rates depending upon the species of alkanes (Figure 3b). Due to the

DOI: 10.1021/acssensors.6b00018
ACS Sens. 2016, 1, 552−559

mechanism of interruption to the PCT by alkanes adsorbed at the D−A interface, the photocurrent change should be temporary with the alkane molecule desorption. Therefore, the alkane length also controls the photocurrent recovery rates. To quantitatively compare them, different alkane recovery curves were fitted with a single exponential function with good correlation and the recovery time is indexed by the lifetime term, τ (Figure S10). For *n*-hexane, *n*-octane, *n*-decane, and *n*-dodecane, τ is about 1.7, 3.5, 4.4, and 11 s, respectively. This variation of photocurrent recovery kinetics supports the disassociation abilities of the different alkanes at the alkyl interface of ACTC/PTCDI-DD composite. Considering the vaporization process of the alkanes from their liquid phase, they disassociate from the homogeneous top layer of the liquid phase, just as the case here in which alkanes disassociate from the alkyl interface of the ACTC/PTCDI-DD composite. For the vaporization process, when the partial pressure does not reach the saturated vapor pressure (P_{sat}), the disassociation process is dominant. Therefore, P_{sat} could describe the general disassociation ability of molecules from an analogous interface. For example, if the P_{sat} is low, the dissociation should be hard and slow. So, we listed the τ value and P_{sat} for each alkane to demonstrate the close connection of these two terms (Table S1). Additionally, it is noted that for the alkane vapors at lower concentrations, the recovery kinetics were maintained even though the amplitudes of the response were much smaller (Figures S8 and S9b). These results indicate that the kinetic characteristics are caused by the thermodynamic nature of alkanes themselves, and are an important fingerprint to further distinguish specific alkanes. The principle component analysis (PCA) method was applied to quantitatively analyze the photocurrent responses curves for the four alkanes (Figure S11 for methods). The principal component scores show compact clustering for same alkanes and clear separations for different alkanes (Figure 3c). Therefore, the sensor has the potential to distinguish different alkanes by applying the PCA method to the sensing data. With reproducible test conditions and standardized compound library, the sensor could help to determine the specific alkanes. Then, combined with signal amplitude, we could finally ensure the kind and concentration of detected alkanes.

The structure of the tunable D−A interface plays a critical role of transmitting the alkane adsorption to photocurrent change in the coassembled ACTC/PTCDI-DD composite. We confirmed this mechanism by two control samples, which lost the sensing performance without the desired interface even though the same materials were used. In the first control experiment, the PTCDI-DD nanofibers and the ACTC nanofibers were prepared separately via solution-based methods and then mechanically mixed to a visually homogeneous state[18,28] (Figure 4a). However, in the microscopic scale, their shapes did not significantly change after the mixing, and the PTCDI-rich part and ACTC-rich part are segregated by obvious boundaries, leading to a very low PCT efficiency. To improve this situation, we drop-cast a solution of ACTC onto PTCDI-DD nanofibers that were already deposited on a substrate. This method was previously used to fabricate highly photoconductive structures with high yield of charge transfer.[17,18] The morphology clearly indicated that the PTCDI-DD nanofibers retained their structures after surface coating and ACTC formed a uniform dense film on the surface of the PTCDI-DD nanofibers (Figure 4b). As expected, this ACTC drop-cast composite shows a remarkable photocurrent

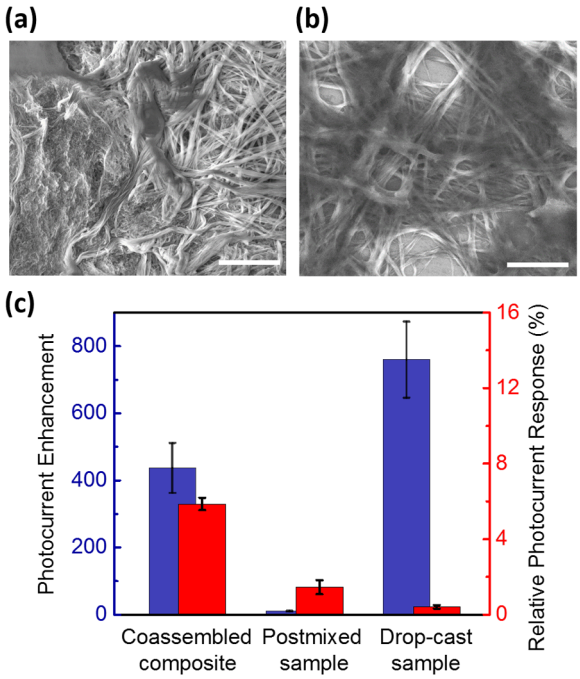

Figure 4. (a) Postmixture of PTCDI-DD nanofibers and ACTC nanofibers; (b) PTCDI-DD nanofibers covered by subsequently drop-cast ACTC molecules; scale bar = 5 μm. (c) Comparison of the relative photocurrent responses upon exposure to saturated vapor of dodecane (red) and photocurrent enhancements (blue) among the three morphologies of the ACTC/PTCDI-DD composites.

enhancement compared to the postmixed sample (Figure S13a). Then we compared the sensing performance of the coassembled, postmixed, and drop-cast samples horizontally. It was found that the order of response of hexane to dodecane in each sample is the same and the overall sensing performance follows the order coassembled sample ≫ postmixed one > drop-cast one. Accordingly, their photocurrent enhancement and responses to dodecane are compared to discuss the tunable D−A interface impact on the sensing performance (Figure 4c). Considering the morphology, the low PCT efficiency and weak response to alkanes of the postmixed sample should be due to the phase separation, specifically, the already interrupted D−A interface (Figure S12b). Therefore, the interruption to the D−A interface contributed from alkanes is very minor. On the other hand, the drop-cast sample performed even worse, which is likely caused by the nonporous ACTC film (Figure S13b). Although the ACTC coating helps to improve the D−A contact, the dense coating reduced the porosity of the PTCDI nanofiber film, likely blocking the small pores and shrinking the larger ones, which seriously deteriorated the vapor access of alkanes at the D−A interface. Without enough molecules to reach the D−A interface, the failure of sensing is expected. In contrast, the coassembled composite demonstrated the largest sensing response, mainly due to the optimal D−A interface, which not only possesses the large area D−A contact (affording high photocurrent), but also provides a uniform bulk D−A heterojunction structure consistent with the porosity formed by the coassembly of the ACTC and PTCDI-DD nanofibers, thus maximizing the adsorption of alkanes at the D−A interface.

The exposures of common solvent vapors mainly increase the photocurrent of ACTC/PTCDI-DD composite in different yields, whose responses are reversed to alkanes (Figure 5 and

DOI: 10.1021/acssensors.6b00018
ACS Sens. 2016, 1, 552−559

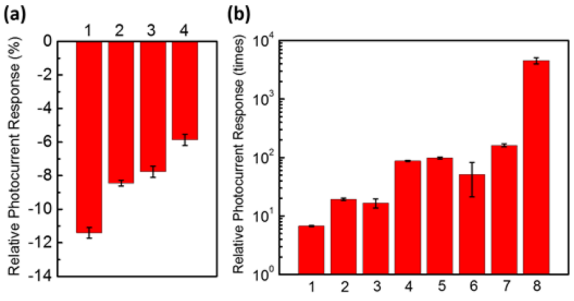

Figure 5. General selectivity of the ACTC/PTCDI-DD composite sensor. The bars in each column represent the relative photocurrent positive response of the ACTC/PTCDI-DD composite to the saturated vapors of (a) (1) *n*-hexane (C_6H_{14}), (2) *n*-octane (C_8H_{18}), (3) *n*-decane ($C_{10}H_{22}$), and (4) *n*-dodecane ($C_{12}H_{26}$); (b) (1) ethanol, (2) acetonitrile, (3) tetrahydrofuran, (4) ethyl acetate, (5) dichloromethane, (6) water, (7) acetone, and (8) hexylamine at room temperature.

S14). This divergence demonstrates the outstanding general selectivity of ACTC/PTCDI-DD composite for alkanes over common solvents. Like alkanes, the adsorption of interferents could also happen at the interface, though it is not optimized for them. With the interfering molecules accumulated at the D−A interface, the charge transfer process might be enhanced by the strong built-in dipole of the interferents, which is also observed in the organic thin film solar cells.[34−36] With greater charge separation, the photocurrent increases during the exposure of the polar interferents (dipole moments listed in Table S2 for reference). Additionally, in some chemicals, the dipole structures may include some electron donating groups, which can directly donate electrons to the PTCDI fiber upon light irradiation.[26] With this additional electron source, the composite achieves an additional two orders greater response than other interferents, as hexylamine here. In contract, due to the nonpolar structures and no electron donating ability, alkane adsorption only enlarges the D−A distance, thus weakening the charge transfer process. Therefore, the difference of dipole moment is likely the origin of the outstanding general selectivity of the ACTC/PTCDI-DD composite.

All above experiments are conducted for vapor detection, but the sensing mechanism does not limit the detection only in gas states. To broaden the application fields and further verify the sensor mechanism, small amounts of liquid of alkanes and interferents were dropped onto the surface of the ACTC/PTCDI-DD composite when the photocurrent was being measured (responses to alkanes in Figure S15 and interferents in Figure S16). Overall, the results for both alkanes and interferents agreed with the trends observed in the vapor exposure experiments, but the amplitudes of photocurrent responses were much larger, owing to the much higher concentrations of analytes at the D−A interface. Within a few seconds after the initial contact, the short chain alkanes (*n*-hexane, cyclohexane, and *n*-octane) evaporated and the photocurrents recovered to the baseline quickly, which demonstrated the robustness of the D−A interface between ACTC and PTCDI-DD nanofibers. In contrast, the recovery for the larger alkanes took a longer time due to their higher boiling points and stronger interaction at the interface.

In summary, the ACTC/PTCDI-DD composite demonstrated outstanding sensitivity and selectivity to alkanes, which result from its compatible and tunable D−A interface. Dodecyl side chains of ACTC and PTCDI-DD help construct the homogeneous D−A interface via solvophilic interaction, and such compatibility also contributes the adsorption of alkanes onto the interface. The coassembly method offers the structural features of large-area but highly porous D−A interface for the ease of interruption by alkanes. These two correlative designs enable the detection of alkanes in both vapor and liquid states. Thanks to the kinetic differences of alkane adsorption and disassociation at the interface, the sensor could further provide selectivity among the different sizes of alkanes. Along with the good general selectivity over the common solvents, the ACTC/PTCDI-DD composite becomes an outstanding candidate of sensing materials for real-world alkane detection. Additionally, the strategy of tuning D−A charge transfer could be a helpful reference for chemical sensor development.

EXPERIMENTAL SECTION

Materials. Alkanes and the interferents, such as *n*-hexane, cyclohexane, *n*-octane, *n*-decane *n*-dodecane, ethanol, acetonitrile, tetrahydrofuran, ethyl acetate, dichloromethane, acetone, and hexylamine, were obtained from Sigma-Aldrich. The nanofiber building block molecules, ACTC, PTCDI-DD, PTCDI-C_6, and PTCDI-PE, were synthesized following previously reported methods.[17,28]

Fabrication of PTCDI, ACTC Nanofibers, and ACTC/PTCDI Nanofibril Composites. ACTC nanofibers, PTCDI nanofibers, and ACTC/PTCDI composites were fabricated using a similar solution-based method as previously published.[22] For single component nanostructures, a 0.1 mM chloroform solution of the building block molecule was prepared. For ACTC/PTCDI composites, the concentration ratios of ACTC and PTCDI were equal to their desired molar ratios and the sum concentration was fixed at 0.2 mM in chloroform solution. One milliliter of the prepared solution was quickly added to 9 mL of ethanol at room temperature while shaking. Then, the oversaturated solution was kept at 4 °C for 12 h. Some reddish (for PTCDI and ACTC/PTCDI) and pale white (for ACTC) aggregates formed at the bottom of the test tubes. The top clear solution (ca. 9 mL) was carefully removed from the test tubes, leaving the samples in ca. 1 mL solvent. The remaining materials were shaken to form a quasi-uniform mixture, which was ready to be transferred to substrates or electrodes.

SEM Characterization. The above prepared materials were drop-cast onto silicon wafers and left in a vacuum oven to dry at room temperature. The SEM characterization was performed with an FEI Nova Nano 630 (FEI Corporation) equipped with a helix detector. All images were captured in the immersion mode in low-vacuum mode (with 0.43 Torr water pressure).

Photocurrent Enhancement Measurement. The photocurrent measurements in Figure 2c,f,i, and Figure S4, Figure S12a, and Figure S13a were carried out using a two-probe method on a Signatone S-1160 Probe Station combined with an Agilent 4156C Precision Semiconductor Parameter Analyzer. The measurements took place in a shielded dark box to eliminate unwanted light and electromagnetic radiation. The electrodes were fabricated using photolithography on a silicon wafer covered with a 300 nm SiO_2 layer. The gold electrode pair was 15 μm in width and 5 μm in gap, and fully covered with the sensor materials via drop-casting. A tungsten lamp (Quartzline, 21 V, 150W) was used as the light source for the photocurrent enhancement measurement. The light was guided by an optical fiber and the intensity reaching the sample surface was 60 mW·cm^{-2}, as measured by a Melles Griot broadband power/energy meter (model: 13PEM001).

Vapor and Liquid Sensing Measurement. The electrodes used in the sensing experiment were interdigitated electrodes fabricated on a quartz wafer, with 20 fingers on each electrode. Each gold electrode pair was about 5 mm in total width, 100 μm in gap. The total area was about 5 mm × 5 mm in size. For ACTC/PTCDI composites, about 0.2 mL of the quasi-uniform mixture was drop-cast onto the electrode and dried in a vacuum oven at room temperature. For the postmixed composite, 1 mL of the quasi-uniform PTCDI nanofiber suspension

DOI: 10.1021/acssensors.6b00018
ACS Sens. 2016, 1, 552−559

and 0.5 mL ACTC nanofiber suspension were mixed and shaken for 4 h. Then ca. 0.3 mL of the postmixture was drop-cast and dried on an electrode with a similar procedure. For the ACTC drop-cast composite, about 0.2 mL of quasi-uniform PTCDI nanofibers was drop-cast and dried on an electrode. Then 0.1 mL of 0.1 mM ACTC chloroform solution was drop-cast on the PTCDI nanofiber layer. The composite was dried in a vacuum oven at room temperature. After the deposition, the electrodes were connected to an Agilent 4156C Precision Semiconductor Parameter Analyzer for photocurrent measurement. The electrode was fixed in a transparent holder, and was kept 5 cm away from the optical-fiber head, which delivered visible light from a tungsten lamp (Fiber-Lite Fiber Optic Illuminator model 190, Dolan-Jenner Industries, Lawrence, MA, 01843). The illumination intensity on the electrode was set at ~20 $mW{\cdot}cm^{-2}$. In a typical vapor preparation, 50 mL of pure liquid was sealed in a 4 L amber glass bottle for 1 day at room temperature to reach the liquid−vapor equilibrium state. Before the measurement, the vapor was removed with a 50 mL glass syringe with a 20 cm metal needle. The vapor was also diluted with the same syringe by mixing dry air. The syringe was mounted to a syringe pump (Model: NE-4000, New Era Pump System. Inc.) and fitted with a 5 mm needle. The needle end was fixed 1 cm away from the top of the electrode by a holder. In an alkane exposure test, 5 mL of vapor was pumped from the syringe at a speed of 110 $mL{\cdot}min^{-1}$, so each exposure time is ca. 3 s. The next exposure occurs 1 min after the previous exposure. In the liquid sensing experiment, an Eppendort Reference Physio Care pipet was used to transfer 5 μL of pure liquid onto the surface of the nanofibers quickly.

■ ASSOCIATED CONTENT

Supporting Information

The Supporting Information is available free of charge on the ACS Publications website at DOI: 10.1021/acssensors.6b00018.

Morphological and solid absorption characterization of ACTC and the three ACTC/PTCDI composites; photoinduced charge transfer study on the three ACTC/PTCDI composites; sensing performance of ACTC/PTCDI-DD composite; PCA method; photoconductivity and sensing performance of control composites; general selectivity and liquid alkanes and solvents test of ACTC/PTCDI-DD composite; photocurrent recovery fitting results for different alkanes and their saturated vapor pressures; dipole moments of alkanes and solvents at room temperature (PDF)

■ AUTHOR INFORMATION

Corresponding Author

*E-mail: lzang@eng.utah.edu.

Present Address

§Department of Chemistry, Sam Houston State University, P.O. Box 2117, Huntsville, TX 77341, USA.

Author Contributions

C. W. synthesized the PTCDI molecules, fabricated the samples, obtained the optical and SEM images, performed all electrical experiments, and drafted the manuscript. B. R. B. edited the manuscript. M. X. performed the fluorescence quenching measurements. N. W. assisted with the vapor testing setup. X. Y. cast the theoretical calculations for the molecules. D. E. G synthesized the ACTC molecule. L. Z. revised the manuscript and supervised the work.

Notes

The authors declare the following competing financial interest(s): Some results have been included in an invention disclosure submitted to the technology and venture commercialization, University of Utah (ID: U-6046) and a related provisional patent application has been submitted.

■ ACKNOWLEDGMENTS

This work was supported by funding from the NSF (CHE 0931466) and the Department of Homeland Security, Science and Technology Directorate under grant number (2009-ST-108-LR0005). B. R. B. is grateful for support from the NASA Office of the Chief Technologist (NNX12AM67H) and NSF IGERT (DGE0903715). We thank Dr. Greger Andersson for the help on the PCA data analysis and Dr. Jeffery S. Moore for the help on synthesis of ACTC.

■ REFERENCES

(1) Matsui, H.; Lee, J. H. On the Measure of the Relative Detonation Hazards of Gaseous Fuel-Oxygen and Air Mixtures. *Symp. Combust., [Proc.]* **1979**, *17*, 1269−1280.

(2) Agrawal, J. P.; Hodgson, R. *Organic Chemistry of Explosives*; John Wiley & Sons, 2007.

(3) Criteria for a Recommended Standard—Occupational Exposure to Alkanes (C5-C8), VI. Work Practices; The National Institute for Occupational Safety and Health (NIOSH) Criteria Documents No. 77−151d, Centers for Disease Control and Prevention, GA, USA, 1977.

(4) Reno, J.; Marcus, D.; Leary, M. L.; Thrman, K. M. *Responding to Terrorism Victims: Oklahoma City and Beyond*; U.S. Department of Justice: Washington, DC, 2000.

(5) Criteria for a Recommended Standard—Occupational Exposure to Alkanes (C5-C8), III. Biologic Effects of Exposure; The National Institute for Occupational Safety and Health (Niosh) Criteria Documents No. 77−151b, Centers for Disease Control and Prevention, GA, USA, 1977.

(6) Chang, Y. C. Neurotoxic Effects of N-Hexane on the Human Central Nervous System: Evoked Potential Abnormalities in N-Hexane Polyneuropathy. *J. Neurol., Neurosurg. Psychiatry* **1987**, *50*, 269−274.

(7) Huang, J.; Kato, K.; Shibata, E.; Sugimura, K.; Hisanaga, N.; Ono, Y.; Takeuchi, Y. Effects of Chronic N-Hexane Exposure on Nervous System-Specific and Muscle-Specific Proteins. *Arch. Toxicol.* **1989**, *63*, 381−385.

(8) Caygill, J. S.; Davis, F.; Higson, S. P. J. Current Trends in Explosive Detection Techniques. *Talanta* **2012**, *88*, 14−29.

(9) Carotta, M. C.; Guidi, V.; Martinelli, G.; Nagliati, M.; Puzzovio, D.; Vecchi, D. Sensing of Volatile Alkanes by Metal-Oxide Semiconductors. *Sens. Actuators, B* **2008**, *130*, 497−501.

(10) Wang, F.; Swager, T. M. Diverse Chemiresistors Based Upon Covalently Modified Multiwalled Carbon Nanotubes. *J. Am. Chem. Soc.* **2011**, *133*, 11181−11193.

(11) Allen, B. L.; Kichambare, P. D.; Star, A. Carbon Nanotube Field-Effect-Transistor-Based Biosensors. *Adv. Mater.* **2007**, *19*, 1439−1451.

(12) Kauffman, D. R.; Star, A. Carbon Nanotube Gas and Vapor Sensors. *Angew. Chem., Int. Ed.* **2008**, *47*, 6550−6570.

(13) Snow, E. S.; Perkins, F. K.; Robinson, J. A. Chemical Vapor Detection Using Single-Walled Carbon Nanotubes. *Chem. Soc. Rev.* **2006**, *35*, 790−798.

(14) Clarke, T. M.; Durrant, J. R. Charge Photogeneration in Organic Solar Cells. *Chem. Rev.* **2010**, *110*, 6736−6767.

(15) Prasanthkumar, S.; Ghosh, S.; Nair, V. C.; Saeki, A.; Seki, S.; Ajayaghosh, A. Organic Donor−Acceptor Assemblies Form Coaxial P−N Heterojunctions with High Photoconductivity. *Angew. Chem., Int. Ed.* **2015**, *54*, 946−950.

(16) López-Andarias, J.; Rodriguez, M. J.; Atienza, C.; López, J. L.; Mikie, T.; Casado, S.; Seki, S.; Carrascosa, J. L.; Martín, N. Highly Ordered N/P-Co-Assembled Materials with Remarkable Charge Mobilities. *J. Am. Chem. Soc.* **2015**, *137*, 893−897.

(17) Che, Y.; Huang, H.; Xu, M.; Zhang, C.; Bunes, B. R.; Yang, X.; Zang, L. Interfacial Engineering of Organic Nanofibril Heterojunctions

DOI: 10.1021/acssensors.6b00018
ACS Sens. 2016, 1, 552−559

into Highly Photoconductive Materials. *J. Am. Chem. Soc.* **2011**, *133*, 1087−1091.
(18) Huang, H.; Chou, C.-E.; Che, Y.; Li, L.; Wang, C.; Yang, X.; Peng, Z.; Zang, L. Morphology Control of Nanofibril Donor−Acceptor Heterojunction to Achieve High Photoconductivity: Exploration of New Molecular Design Rule. *J. Am. Chem. Soc.* **2013**, *135*, 16490−16496.
(19) Yiu, A. T.; Beaujuge, P. M.; Lee, O. P.; Woo, C. H.; Toney, M. F.; Fréchet, J. M. J. Side-Chain Tunability of Furan-Containing Low-Band-Gap Polymers Provides Control of Structural Order in Efficient Solar Cells. *J. Am. Chem. Soc.* **2012**, *134*, 2180−2185.
(20) Holcombe, T. W.; Norton, J. E.; Rivnay, J.; Woo, C. H.; Goris, L.; Piliego, C.; Griffini, G.; Sellinger, A.; Brédas, J.-L.; Salleo, A.; Fréchet, J. M. J. Steric Control of the Donor/Acceptor Interface: Implications in Organic Photovoltaic Charge Generation. *J. Am. Chem. Soc.* **2011**, *133*, 12106−12114.
(21) Chen, S.; Wang, C.; Bunes, B. R.; Li, Y.; Wang, C.; Zang, L. Enhancement of Visible-Light-Driven Photocatalytic H2 Evolution from Water over G-C3n4 through Combination with Perylene Diimide Aggregates. *Appl. Catal., A* **2015**, *498*, 63−68.
(22) Zang, L.; Che, Y.; Moore, J. S. One-Dimensional Self-Assembly of Planar Π-Conjugated Molecules: Adaptable Building Blocks for Organic Nanodevices. *Acc. Chem. Res.* **2008**, *41*, 1596−1608.
(23) Briseno, A. L.; Mannsfeld, S. C. B.; Reese, C.; Hancock, J. M.; Xiong, Y.; Jenekhe, S. A.; Bao, Z.; Xia, Y. Perylenediimide Nanowires and Their Use in Fabricating Field-Effect Transistors and Complementary Inverters. *Nano Lett.* **2007**, *7*, 2847−2853.
(24) Chen, S.; Slattum, P.; Wang, C.; Zang, L. Self-Assembly of Perylene Imide Molecules into 1d Nanostructures: Methods, Morphologies, and Applications. *Chem. Rev.* **2015**, *115*, 11967−11998.
(25) Jones, B. A.; Facchetti, A.; Wasielewski, M. R.; Marks, T. J. Tuning Orbital Energetics in Arylene Diimide Semiconductors. Materials Design for Ambient Stability of N-Type Charge Transport. *J. Am. Chem. Soc.* **2007**, *129*, 15259−15278.
(26) Che, Y.; Yang, X.; Liu, G.; Yu, C.; Ji, H.; Zuo, J.; Zhao, J.; Zang, L. Ultrathin N-Type Organic Nanoribbons with High Photoconductivity and Application in Optoelectronic Vapor Sensing of Explosives. *J. Am. Chem. Soc.* **2010**, *132*, 5743−5750.
(27) Zang, L. Interfacial Donor−Acceptor Engineering of Nanofiber Materials to Achieve Photoconductivity and Applications. *Acc. Chem. Res.* **2015**, *48*, 2705−2714.
(28) Naddo, T.; Che, Y.; Zhang, W.; Balakrishnan, K.; Yang, X.; Yen, M.; Zhao, J.; Moore, J. S.; Zang, L. Detection of Explosives with a Fluorescent Nanofibril Film. *J. Am. Chem. Soc.* **2007**, *129*, 6978−6979.
(29) Liao, Q.; Fu, H.; Wang, C.; Yao, J. Cooperative Assembly of Binary Molecular Components into Tubular Structures for Multiple Photonic Applications. *Angew. Chem., Int. Ed.* **2011**, *50*, 4942−4946.
(30) Che, Y.; Datar, A.; Yang, X.; Naddo, T.; Zhao, J.; Zang, L. Enhancing One-Dimensional Charge Transport through Intermolecular Π-Electron Delocalization: Conductivity Improvement for Organic Nanobelts. *J. Am. Chem. Soc.* **2007**, *129*, 6354−6355.
(31) Meager, I.; Ashraf, R. S.; Mollinger, S.; Schroeder, B. C.; Bronstein, H.; Beatrup, D.; Vezie, M. S.; Kirchartz, T.; Salleo, A.; Nelson, J.; McCulloch, I. Photocurrent Enhancement from Diketopyrrolopyrrole Polymer Solar Cells through Alkyl-Chain Branching Point Manipulation. *J. Am. Chem. Soc.* **2013**, *135*, 11537−11540.
(32) Tsuzuki, S.; Matsumoto, H.; Shinoda, W.; Mikami, M. Effects of Conformational Flexibility of Alkyl Chains of Cations on Diffusion of Ions in Ionic Liquids. *Phys. Chem. Chem. Phys.* **2011**, *13*, 5987−5993.
(33) Hoffmann, M. W. G.; Prades, J. D.; Mayrhofer, L.; Hernandez-Ramirez, F.; Järvi, T. T.; Moseler, M.; Waag, A.; Shen, H. Highly Selective Sam−Nanowire Hybrid No2 Sensor: Insight into Charge Transfer Dynamics and Alignment of Frontier Molecular Orbitals. *Adv. Funct. Mater.* **2014**, *24*, 595−602.
(34) Xu, Z.; Chen, L.-M.; Yang, G.; Huang, C.-H.; Hou, J.; Wu, Y.; Li, G.; Hsu, C.-S.; Yang, Y. Vertical Phase Separation in Poly(3-Hexylthiophene): Fullerene Derivative Blends and Its Advantage for Inverted Structure Solar Cells. *Adv. Funct. Mater.* **2009**, *19*, 1227−1234.
(35) Carsten, B.; Szarko, J. M.; Son, H. J.; Wang, W.; Lu, L.; He, F.; Rolczynski, B. S.; Lou, S. J.; Chen, L. X.; Yu, L. Examining the Effect of the Dipole Moment on Charge Separation in Donor−Acceptor Polymers for Organic Photovoltaic Applications. *J. Am. Chem. Soc.* **2011**, *133*, 20468−20475.
(36) Xu, T.; Lu, L.; Zheng, T.; Szarko, J. M.; Schneider, A.; Chen, L. X.; Yu, L. Tuning the Polarizability in Donor Polymers with a Thiophenesaccharin Unit for Organic Photovoltaic Applications. *Adv. Funct. Mater.* **2014**, *24*, 3432−3437.

DOI: 10.1021/acssensors.6b00018
ACS Sens. 2016, 1, 552−559